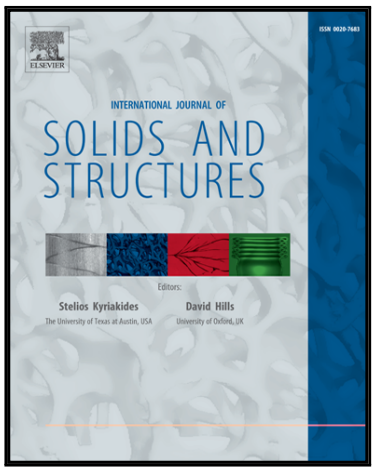

Uncertainty Quantification of Residual Stress Evaluation by the FIB-DIC Ring-Core Method due to Elastic Anisotropy Effects

Enrico Salvati , Tan Sui , Alexander M. Korsunsky

PII: S0020-7683(16)00093-7
DOI: 10.1016/j.ijsolstr.2016.02.031
Reference: SAS 9076

To appear in: *International Journal of Solids and Structures*

Received date: 24 June 2015
Revised date: 5 February 2016
Accepted date: 22 February 2016

Please cite this article as: Enrico Salvati , Tan Sui , Alexander M. Korsunsky , Uncertainty Quantification of Residual Stress Evaluation by the FIB-DIC Ring-Core Method due to Elastic Anisotropy Effects, *International Journal of Solids and Structures* (2016), doi: 10.1016/j.ijsolstr.2016.02.031

Highlights

- Compact matrix formulation is presented for residual stress calculation from residual strains using Voigt's 6-vector notation

- By performing the calculation for 8000 randomly selected crystal orientations, Uncertainty Quantification is obtained of residual stress evaluation for cubic materials with different anisotropy factors

Uncertainty Quantification of Residual Stress Evaluation by the FIB-DIC Ring-Core Method due to Elastic Anisotropy Effects

Enrico Salvati[1], Tan Sui[1], Alexander M. Korsunsky[1]

[1] Multi-Beam Laboratory for Engineering Microscopy (MBLEM), Department of Engineering Science, University of Oxford, Parks Road, Oxford OX1 3PJ, United Kingdom

Corresponding author:

Enrico Salvati

Department of Engineering Science

University of Oxford

Parks Road

Oxford OX1 3PJ

United Kingdom

Tel: +44-18652-83447

Fax: +44-18652-73010

E-Mail: enrico.salvati@eng.ox.ac.uk

Abstract:

Elastic anisotropy can have a significant effect on the reliability and precision of residual stress evaluation, due to the uncertainty in the elastic constants multiplied by the measured strains. For the focused ion beam – digital image correlation (FIB-DIC) ring-core method taken as an example, a Mathematica package was developed to evaluate the complete in-plane residual stress state from the measured strain relief values using known material orientation and anisotropic elastic properties for materials displaying cubic symmetry. However, in many practical situations the underlying material orientation is unknown, and nominal isotropic continuum elastic constants are used. This leads to a systematic error in the stress calculation. The present analysis focuses on the statistical evaluation of the uncertainty in stress evaluation due to the unknown material orientation as a function of its degree of anisotropy. We demonstrate an experimental application of this procedure to a real case of micron scale residual stress analysis in a nickel-base superalloy.

Keywords:

Uncertainty Quantification, Anisotropy, Residual Stress, FIB-DIC

1. Introduction

Residual stresses across the scales

Residual stresses within engineering materials and structures have been the subject of extensive study for many decades, due to their significant influence on the structural integrity and durability of engineering components and structures. For the purposes of analysis, residual stresses have been classified according to the length scale of their variation as macroscopic (Type I) and microscopic, with further distinction being made between Type II intergranular microstresses that vary on the scale of many microns and describe grain interaction, and Type III intra-granular stresses, varying on the short scale within individual crystallites [1-2].

Until recently macroscopic residual stresses were the most well-studied, not simply because of their significance at the structural scale, but also due to the availability of experimental techniques for their measurement that range from X-ray and neutron diffraction to hole drilling. Type II microstresses can be analysed by selective averaging of powder diffraction type data from grains sharing certain crystallographic orientation, which provides very useful, but limited insight into microscopic residual stress state.

Only recently the methods have become available for efficient and fast residual stress evaluation at the intra-granular scale, typically at the scale of microns. Residual stresses at the scale of individual grains are present in polycrystalline aggregates almost always, as a consequence of mechanical constraint provided by the neighbouring crystals, in combination with thermal, elastic and plastic anisotropy.

Experimental techniques capable of attaining micron resolution provide a measure of displacements or strains, followed by stress calculation using the generalised Hooke's law.

Whilst the uncertainty of strain or displacement measurement can be quantified using experimental error analysis methods, the stress calculation introduces further uncertainties that require quantification. In a single grain within an aggregate, the local crystal structure may have a dramatic effect on the stress state due to the orientation of the grain itself and of its neighbouring grains with the respect of external loading. A complex relationship exists between global and local stress-strain states that reflects the accommodation taking place during elastoplastic deformation of a polycrystal, leading to simultaneous attainment of stress equilibrium and strain compatibility [3, 4]. The models in the literature that simulate the local stress evolution [5,6] share a common need for direct experimental validation, emphasising the requirement for correct stress evaluation at the intra-granular level.

FIB-DIC micro-ring-core method

Amongst the various techniques adapted to the measurement of residual stress at the micron scale, the Focused Ion Beam – Digital Image Correlation (FIB-DIC) ring-core method [7,8] is particularly versatile and adaptable [9]. This method may be considered as a semi-destructive technique that is analogous to the macro-scale ring-core method, in that it is based on the measurement of material relief after cutting. The difference stems from the fact that Focused Ion Beam (FIB) is adopted as the milling tool for the material removal, and SEM is used for imaging. In the course of the milling process a circular trench is machined around the central “island”, or micro-pillar. The variation of surface strain in the course of this procedure is monitored using high resolution imaging by means of a Scanning Electron Microscope (SEM) (Fig.1a). Digital Imagine Correlation (DIC) software is used to determine the displacement field, and to compute

the strain increment. The apparent strain relief evolution as a function of milling depth is plotted, the profile is fitted with a "master curve" function [10] derived from Finite Element Modelling (FEM). This procedure allows robust estimation of the residual strain present at the same location prior to milling. The analysis of the strain components, in at least three different in-plane directions, provides enough information for the reconstruction of the complete in-plane strain state. This aspect of the method coupled with the high spatial resolution attainable (on the order of one micron) makes the FIB-DIC ring-core method a particularly good approach to the evaluation of intragranular stress.

Evaluation of stress considering anisotropy

Engineering reliability and durability analysis for design e.g. against creep or high cycle fatigue conventionally uses criteria based on stresses, rather than strains. For isotropic materials the stress calculation can be readily performed using the combination of only two elastic parameters: Young's Modulus E and Poisson's Ratio ν. The aim of this paper is to present and to evaluate the extension of the residual stress calculation in the FIB-DIC ring-core method for the case when the material is anisotropic, and possesses cubic symmetry. The results show that the uncertainty of residual stress evaluation at the inter- and/or intragranular level depends on the material's degree of anisotropy, and that for materials with high anisotropy factor the knowledge of grain orientation is mandatory.

Mathematica procedure

The computational background to the analysis of relief strains in the FIB-DIC micro-ring-core experiments, such as illustrated in Fig.1(a), has been presented in a series of papers [7,8,10]. The central idea of the method that has been validated through extensive numerical modelling is that the surface of the micro-pillar undergoes the change from initial residual elastic strain to the final strain-free state that arises after sufficiently deep milling (to the depth of the order of the pillar diameter, or greater [7]. Therefore, simple inversion of the sign of the perceived strain relief during milling provides a means of determining the pre-existing residual strain. The FIB-DIC ring-core method [9] allows simultaneous evaluation of three components of surface in-plane relief strains ($\Delta\varepsilon_{11}, \Delta\varepsilon_{22}, \Delta\varepsilon_{12}$) (and hence the residual elastic strains) in the laboratory (global) Cartesian system (Fig.1b), The three out-of-plane strain components ($\varepsilon_{33}, \varepsilon_{13}, \varepsilon_{23}$) are not measured in this configuration. However, it can be assumed that the traction-free surface condition prevails, so that the three out-of-plane stress components vanish in the initial state ($\sigma_{33} = \sigma_{13} = \sigma_{23} = 0$). This additional boundary condition allows the out-of-plane residual strain to be also found.

Assuming the grain orientation at the milling location and the elastic properties of the material (stiffness matrix) to be known, a compact analytical procedure can be elaborated for the calculation of the full local stress tensor. To aid the algebraic manipulations, to ensure their correctness and to enable direct use of the resulting expressions for numerical calculation, the procedure is implemented using Mathematica package. Arbitrary materials with cubic symmetry can be considered, with varying degrees of elastic anisotropy. For cubic materials this property of the material can be characterised by a single parameter known as the Zener anisotropy factor [11]. For illustration, Ni-base superalloy is taken as an example of a highly anisotropic crystal, in which the ratio of Young's moduli in the stiffest and most compliant directions is of the order of

2.5. Single crystal silicon is taken as a moderate case for which this ratio is ~1.6. Finally, Al and its alloys are considered as materials that have properties close to isotropic material, with the ratio of stiffnesses ~1.2.

Once the procedure is established and validated, sensitivity analysis is performed to assess the extent to which errors in stress evaluation arise from the ignorance of the underlying crystal orientation, if the assumption of isotropic equivalent stiffness for bulk polycrystal is used. Different strain states are considered, and calculations are carried out for n=8000 instances of randomly distributed grain orientations described by the three Euler angles. Since the selection of Euler angles encompasses the complete range of possibilities, and describes a uniform distribution in the orientation space, this gives unbiased statistical evaluation. The results serve as the basis for uncertainty quantification of stress evaluation using this approach.

Experimental result

The practical implementation and application of the method is illustrated using a set of experimental data for residual stresses in a cross-section of an aeroengine turbine blade made from a Ni-base superalloy, a material with a high Zener anisotropy factor. We present a comparison of the stresses computed assuming correct anisotropic elastic properties against the results obtained assuming that the material is isotropic, and assess the findings.

2. Tensor and 6-vector matrix representation

We first define a Cartesian coordinate system that will be referred to as local, or crystal system of axes, associated with the cubic unit cell of the material. We also define a global, or laboratory system of axes. In absence of grain rotation, the local system is coincident with the global. In this

global system, the x_3 axis is associated with the normal to the sample surface and the x_1 and x_2 axes are associated with suitable mutually orthogonal directions parallel to the sample surface, e.g. the fast and slow scan directions within the SEM system. The graphical representation of these definitions is shown in Fig.1 in which the coordinate systems are distinguished by the subscript L for the local system, and G for global system. In the derivation below all quantities referring to a specific system have appropriate subscripts.

According to the Bunge notation [13], the general rotation between two arbitrary orientations of a crystal can be defined by means of the three Euler angles $(\varphi_1, \Phi, \varphi_2)$. Figure 1(a) illustrates this definition in which the rotation applied to a cubic crystal, initially aligned with the global axes, in order to bring it into alignment with the actual orientation of the local, or crystal axes. Firstly, rotation by the angle φ_1 is applied around axis x_1 , then the rotation by the angle Φ is applied around the new rotated axis $\tilde{x}_3$, and finally the third rotation by the angle φ_2 is applied around the new axis x_1'. The resulting coordinate system is referred to as local, and is associated with the crystal axes denoted x_1', x_2', x_3'.

The matrix that describes the transformation of a vector from a given coordinate system to another one rotated by an angle α_3 around the x_3 axis is given by

$$\bar{v}' = \overline{\overline{\boldsymbol{R}(\alpha_3)}}\,\bar{v}, \quad \overline{\overline{\boldsymbol{R}(\alpha_3)}} = \begin{pmatrix} \mathrm{Cos}[\alpha_3] & \mathrm{Sin}[\alpha_3] & 0 \\ -\mathrm{Sin}[\alpha_3] & \mathrm{Cos}[\alpha_3] & 0 \\ 0 & 0 & 1 \end{pmatrix} \tag{1}$$

Rotation matrices for other angles and axes are obtained by permutation of rows and columns. For example, for the first Euler angle φ_1 the matrix has the form:

$$\overline{\overline{\boldsymbol{R}(\varphi_1)}} = \begin{pmatrix} 1 & 0 & 0 \\ 0 & \mathrm{Cos}[\varphi_1] & \mathrm{Sin}[\varphi_1] \\ 0 & -\mathrm{Sin}[\varphi_1] & \mathrm{Cos}[\varphi_1] \end{pmatrix} \quad (2)$$

The matrix $\overline{\overline{\boldsymbol{R}}}$ that describe the sequence of rotations with respect to different axes is given by the product of rotation matrices for different axes and angles is given by the product of matrices:

$$\overline{\overline{\boldsymbol{R}}} = \overline{\overline{\boldsymbol{R}(\varphi_1, \Phi, \varphi_2)}} = \overline{\overline{\boldsymbol{R}(\varphi_2)}} . \overline{\overline{\boldsymbol{R}(\Phi)}} . \overline{\overline{\boldsymbol{R}(\varphi_1)}} \quad (3)$$

In the Bunge notation this rotation matrix $\overline{\overline{\boldsymbol{R}}}$ from the global to the local coordinate system is expressed explicitly as follows:

$$\overline{\overline{\boldsymbol{R}}} = \begin{pmatrix} \mathrm{Cos}[\varphi_1]\mathrm{Cos}[\varphi_2] - \mathrm{Cos}[\Phi]\mathrm{Sin}[\varphi_1]\mathrm{Sin}[\varphi_2] & \mathrm{Cos}[\varphi_2]\mathrm{Sin}[\varphi_1] + \mathrm{Cos}[\varphi_1]\mathrm{Cos}[\Phi]\mathrm{Sin}[\varphi_2] & \mathrm{Sin}[\varphi_2]\mathrm{Sin}[\Phi] \\ -\mathrm{Cos}[\varphi_2]\mathrm{Cos}[\Phi]\mathrm{Sin}[\varphi_1] - \mathrm{Cos}[\varphi_1]\mathrm{Sin}[\varphi_2] & \mathrm{Cos}[\varphi_1]\mathrm{Cos}[p]\mathrm{Cos}[\Phi] - \mathrm{Sin}[\varphi_1]\mathrm{Sin}[\varphi_2] & \mathrm{Cos}[\varphi_2]\mathrm{Sin}[\Phi] \\ \mathrm{Sin}[\varphi_1]\mathrm{Sin}[\Phi] & -\mathrm{Cos}[\varphi_1]\mathrm{Sin}[\Phi] & \mathrm{Cos}[\Phi] \end{pmatrix} \quad (4)$$

Tensor transformation between the global and local coordinate axes systems (indicated by the subscripts *G* and *L* respectively) is accomplished by pre- and post-multiplication by the rotation matrix and its transpose. For example, for the stress tensor the transformation is expressed as:

$$\overline{\overline{\boldsymbol{\sigma_L}}} = \overline{\overline{\boldsymbol{R}}}\ \overline{\overline{\boldsymbol{\sigma_G}}}\ \overline{\overline{\boldsymbol{R^T}}} \quad (5)$$

Exactly the same transformation applies to the strain tensor defined in the consistent tensorial form, $\varepsilon_{ij} = \frac{1}{2}\left(\frac{\partial u_i}{\partial x_j} + \frac{\partial u_j}{\partial x_i}\right)$:

$$\overline{\overline{\boldsymbol{\varepsilon_L}}} = \overline{\overline{\boldsymbol{R}}}\ \overline{\overline{\boldsymbol{\varepsilon_G}}}\ \overline{\overline{\boldsymbol{R^T}}} . \quad (6)$$

Since the reverse rotation matrix is described by $\overline{\overline{\boldsymbol{R^{-1}}}} = \overline{\overline{\boldsymbol{R^T}}}$, the backward rotation is expressed as

$$\overline{\overline{\boldsymbol{\varepsilon_G}}} = \overline{\overline{\boldsymbol{R^T}}}\ \overline{\overline{\boldsymbol{\varepsilon_L}}}\ \overline{\overline{\boldsymbol{R}}} \quad (7)$$

The relationship between strains and stresses in linear elasticity is expressed in the form of the generalised Hooke's law. The elastic properties are described by the stiffness tensor $\widetilde{\boldsymbol{C}}$, or its reciprocal compliance tensor $\widetilde{\boldsymbol{S}}$, where the tilde sign denotes the fourth order tensor:

$$\overline{\overline{\boldsymbol{\sigma_L}}} = \widetilde{\boldsymbol{C}} : \overline{\overline{\boldsymbol{\varepsilon_L}}}, \qquad \overline{\overline{\boldsymbol{\varepsilon_L}}} = \widetilde{\boldsymbol{S}} : \overline{\overline{\boldsymbol{\sigma_L}}} \ . \tag{8}$$

In practice these relationships are reported in the literature for different materials in reference to the Cartesian crystal axes associated with the lattice unit cell. However, not only is the fourth order tensor notation somewhat unwieldy, it also does not take into account explicitly the general symmetry properties of stiffness and compliance coefficients. For this reason elasticity relations are usually reported in the form of matrices using the 6-vector Voigt notation for stresses and strains [12]:

$$\bar{\boldsymbol{\varepsilon}} = (\varepsilon_{11}, \varepsilon_{22}, \varepsilon_{22}, 2\varepsilon_{23}, 2\varepsilon_{13}, 2\varepsilon_{12}), \qquad \bar{\boldsymbol{\sigma}} = (\sigma_{11}, \sigma_{22}, \sigma_{33}, \sigma_{23}, \sigma_{13}, \sigma_{12}). \tag{9}$$

Using this basis, and adopting the notation $\gamma_{ij} = 2\varepsilon_{ij}$ for shear strains ($i \neq j$), the relationship between strain and stress for a general anisotropic material with respect to the local coordinate system is written using the 6×6 *compliance matrix* as follows:

$$\begin{pmatrix} e_{11} \\ e_{22} \\ e_{33} \\ g_{23} \\ g_{13} \\ g_{12} \end{pmatrix}_G = \begin{pmatrix} S_{11} & S_{12} & S_{13} & S_{14} & S_{15} & S_{16} \\ S_{12} & S_{22} & S_{23} & S_{24} & S_{25} & S_{26} \\ S_{13} & S_{23} & S_{33} & S_{34} & S_{35} & S_{36} \\ S_{14} & S_{24} & S_{34} & S_{44} & S_{45} & S_{46} \\ S_{15} & S_{25} & S_{35} & S_{45} & S_{55} & S_{56} \\ S_{16} & S_{26} & S_{36} & S_{46} & S_{56} & S_{66} \end{pmatrix}_G \begin{pmatrix} s_{11} \\ s_{22} \\ s_{33} \\ t_{23} \\ t_{13} \\ t_{12} \end{pmatrix}_G \tag{10}$$

or in short:

$$\bar{\boldsymbol{\varepsilon}}_{\boldsymbol{L}} = \bar{\bar{\boldsymbol{S}}}\bar{\boldsymbol{\sigma}}_{\boldsymbol{L}} \ . \tag{11}$$

Note the single overbar indicating the vector notation for stresses and strains, and the double overbar indicating the fact that compliance is described by the square matrix. The inverse form of this relationship may also be written using the stiffness matrix

$$\bar{\boldsymbol{\sigma}}_{\boldsymbol{L}} = \bar{\bar{\boldsymbol{C}}}\,\bar{\boldsymbol{\varepsilon}}_{\boldsymbol{L}}, \qquad \bar{\bar{\boldsymbol{C}}} = \bar{\bar{\boldsymbol{S}}}^{-\mathbf{1}} \ . \tag{12}$$

The compact nature of the 6-vector notation brings with it significant advantages, but also leads to some complications. Firstly, the stiffness and compliance matrices under coordinate system rotation no longer obey the simple rules derived from simple 3-vector rotation. Furthermore, the introduction of the coefficient 2 for shear strains destroys the similarity of description for stress and strain 6-vectors, so that the rotation rules for these two fundamental quantities are no longer the same. As a consequence, the transformation rules for the stiffness and compliance matrices are complex, counter-intuitive, and are likely to contain errors if derived by hand and transcribed to and from a printed page. This may be the reason why, to the best of the authors' knowledge, these transformation rules have not been widely reported in the literature.

Modern capabilities of data storage and transmission and the combination of symbolic and numeric manipulation suggest that the most rational means for these algorithms to be derived and made available to the reader is in the form of computer code. To this end we present the implementation of these procedures in a Mathematica® notebook that is made available to the reader as Supplementary Material alongside the present article.

The algorithm implemented in the code is as follows:

1. Tensor rotation matrix $\overline{\overline{\boldsymbol{R}}}$ is computed symbolically using eq. (3) in terms of the trigonometric functions of the Euler angles.
2. Component-wise definitions are introduced for the stress tensor $\overline{\overline{\boldsymbol{\sigma}}}$ and the strain tensor $\overline{\overline{\boldsymbol{\varepsilon}}}$.
3. In preparation for the use of Voigt 6-vector notation, definitions of the stress vector $\overline{\boldsymbol{\sigma}}$ and the strain vector $\overline{\boldsymbol{\varepsilon}}$ are introduced in terms of the same components, including the factor 2 for shear strains.
4. The 'forward' stress tensor transformation from the global to the local coordinate axes is computed symbolically using eq. (5).
5. Using the command for determining the coefficients of vector components in a given expression, six coefficients of six distinct components of the original stress tensor are determined for the six distinct stress components of the transformed tensor.
6. The results are assembled into a '6-stress forward rotation matrix' $\overline{\overline{\boldsymbol{R_\sigma}}}$ that accomplishes the following linear operation:

$$\overline{\boldsymbol{\sigma_L}} = \overline{\overline{\boldsymbol{R_\sigma}}}\ \overline{\boldsymbol{\sigma_G}} \tag{13}$$

7. The above six steps are repeated in order to obtain the symbolic expression for the '6-strain forward rotation matrix' that accomplishes the following linear operation:

$$\overline{\boldsymbol{\varepsilon_L}} = \overline{\overline{\boldsymbol{R_\varepsilon}}}\ \overline{\boldsymbol{\varepsilon_G}} \tag{14}$$

8. It is noted, and verified, that in a similar way the '6-stress inverse rotation matrix' $\overline{\overline{\boldsymbol{R_\sigma^{-1}}}}$ and the '6-strain inverse rotation matrix' $\overline{\overline{\boldsymbol{R_\varepsilon^{-1}}}}$ can be derived, and that they are given by the matrix inverses of their 'forward' counterparts:

$$\overline{\boldsymbol{\sigma_G}} = \overline{\overline{\boldsymbol{R_\sigma^{-1}}}}\,\overline{\boldsymbol{\sigma_L}}, \qquad \overline{\boldsymbol{\varepsilon_G}} = \overline{\overline{\boldsymbol{R_\varepsilon^{-1}}}}\ \overline{\boldsymbol{\varepsilon_L}}. \tag{15}$$

9. The transformation rules for the stiffness and compliance 6×6 matrices are derived in the following form:

$$\overline{\boldsymbol{\sigma_G}} = \overline{\overline{\boldsymbol{R_\sigma^{-1}}}}\,\overline{\boldsymbol{\sigma_L}} = \overline{\overline{\boldsymbol{R_\sigma^{-1}}}}\,\overline{\overline{\boldsymbol{C}}}\,\overline{\boldsymbol{\varepsilon_L}} = \overline{\overline{\boldsymbol{R_\sigma^{-1}}}}\,\overline{\overline{\boldsymbol{C}}}\,\overline{\overline{\boldsymbol{R_\varepsilon}}}\,\overline{\boldsymbol{\varepsilon_G}}\,, \tag{16}$$

and therefore

$$\overline{\overline{\boldsymbol{C_G}}} = \overline{\overline{\boldsymbol{R_\sigma^{-1}}}}\,\overline{\overline{\boldsymbol{C}}}\,\overline{\overline{\boldsymbol{R_\varepsilon}}}\,. \tag{17}$$

Here subscript *G* denotes that the stiffness matrix is now referred to the global axes.

10. Similar reasoning leads to the expression for the compliance matrix referred to the global axes:

$$\overline{\overline{\boldsymbol{S_G}}} = \overline{\overline{\boldsymbol{R_\varepsilon^{-1}}}}\,\overline{\overline{\boldsymbol{S}}}\,\overline{\overline{\boldsymbol{R_\sigma}}}\,. \tag{18}$$

The resulting formulae run to many lines which will not be transcribed here. Instead, the reader is referred to Supplementary Materials for a chance to test the derived transformation rules, and verify their validity.

3. Application of transformation rules for stress determination from FIB-DIC data

In the previous section the expressions were derived in symbolic form for the stiffness and compliance tensors in the global coordinate system after rotation of a material volume with cubic elastic symmetry by an arbitrary set of Euler angles. Since these expressions are obtained within a symbolic and numerical computational framework, a further step can be made towards statistical analysis of stress interpretation in situations that involve anisotropic elasticity calculations.

In the case of FIB-DIC ring-core method, the gauge volume at the milling location lies at the free surface. We therefore make the assumption that, in the residually stressed state prior to milling, the deformed state corresponds to plane stress. It may be noted further that numerical experiments demonstrate that greatest contribution to the overall strain change during ring-core milling (~70%) is made by the residual stress at depths less than one third of the core diameter [14]. Therefore, the out-of plane stress components are ignored in the analysis of materials stress state:

$$\sigma_{33} = \tau_{13} = \tau_{23} = 0. \tag{19}$$

The in-plane strain components present in the residually stressed state at the measurement location are found from the experimentally measured relief strains during FIB-DIC ring-core procedure. Therefore, the overall strain-stress relationship written in the global axes as:

$$\begin{pmatrix} \varepsilon_{11} \\ \varepsilon_{22} \\ \varepsilon_{33} \\ \gamma_{23} \\ \gamma_{31} \\ \gamma_{12} \end{pmatrix}_G = \begin{pmatrix} S_{11} & S_{12} & S_{13} & S_{14} & S_{15} & S_{16} \\ S_{12} & S_{22} & S_{23} & S_{24} & S_{25} & S_{26} \\ S_{13} & S_{23} & S_{33} & S_{34} & S_{35} & S_{36} \\ S_{14} & S_{24} & S_{34} & S_{44} & S_{45} & S_{46} \\ S_{15} & S_{25} & S_{35} & S_{45} & S_{55} & S_{56} \\ S_{16} & S_{26} & S_{36} & S_{46} & S_{56} & S_{66} \end{pmatrix}_G \begin{pmatrix} \sigma_{11} \\ \sigma_{22} \\ 0 \\ 0 \\ 0 \\ \tau_{12} \end{pmatrix}_G \tag{20}$$

is reduced to

$$\begin{pmatrix} \varepsilon_{11} \\ \varepsilon_{22} \\ \gamma_{12} \end{pmatrix}_G = \begin{pmatrix} S_{11} & S_{12} & S_{16} \\ S_{12} & S_{22} & S_{26} \\ S_{16} & S_{26} & S_{66} \end{pmatrix}_G \begin{pmatrix} \sigma_{11} \\ \sigma_{22} \\ \tau_{12} \end{pmatrix}_G \tag{21}$$

For compactness this relationship can be written as:

$$\overline{\boldsymbol{\varepsilon_G}^*} = \overline{\overline{\boldsymbol{S_G}^*}}\ \overline{\boldsymbol{\sigma_G}^*} \tag{22}$$

Here $\overline{\varepsilon_G^*}$ is the reduced 3-vector of in-plane strain components extracted from the FIB-DIC ring-core measurements, $\overline{\overline{S_G^*}}$ is the reduced 3×3 compliance matrix, and $\overline{\sigma_G^*}$ is the 3-vector of stress containing only the in-plane components. The inversion of (22) allows the unknown 3-vector $\overline{\sigma_G^*}$ to be found as:

$$\overline{\boldsymbol{\sigma_G}^*} = \overline{\overline{\boldsymbol{S_G}^*}}^{-1}\ \overline{\boldsymbol{\varepsilon_G}^*} \tag{23}$$

The stress 6-vector $\bar{\boldsymbol{\sigma}}$ in the global system is now completely known. Therefore, its back-substitution in eq.(20) allows the determination of the unmeasured out-of-plane strain components ε_{33}, γ_{23}, γ_{13}.

4. Uncertainty Quantification of stress determination from FIB-DIC ring-core data

Procedure and examples

The residual stress evaluated using FIB-DIC and the subsequently adopted mathematical procedure described above can now be applied to the analysis of single crystals with anisotropic elastic properties. A statistical analysis of the results of residual stress determination can be conducted. In the present study we consider a set of *n* = 8000 cubic crystals of randomly and evenly distributed orientation. Since the output given of FIB-DIC ring-core method is the set of three in-plane strains, in this analysis we consider three representative cases: (a) uniaxial strain state; (b) equi-biaxial strain state where the two normal components of strain are non-zero and

equal, while the shear strain is zero, and (c) a strain state for which one normal strain is twice the magnitude of the other, whilst the shear strain is zero.

For materials with cubic structure the generalised Hooke's law takes the form:

$$\begin{pmatrix} \sigma_{11} \\ \sigma_{22} \\ \sigma_{33} \\ \tau_{23} \\ \tau_{31} \\ \tau_{12} \end{pmatrix}_L = \begin{pmatrix} C_{11} & C_{12} & C_{12} & 0 & 0 & 0 \\ C_{12} & C_{11} & C_{12} & 0 & 0 & 0 \\ C_{12} & C_{12} & C_{11} & 0 & 0 & 0 \\ 0 & 0 & 0 & C_{44} & 0 & 0 \\ 0 & 0 & 0 & 0 & C_{44} & 0 \\ 0 & 0 & 0 & 0 & 0 & C_{44} \end{pmatrix}_L \begin{pmatrix} \varepsilon_{11} \\ \varepsilon_{22} \\ \varepsilon_{33} \\ \gamma_{23} \\ \gamma_{31} \\ \gamma_{12} \end{pmatrix}_L \tag{24}$$

The influence of the degree of anisotropy on stress determination from FIB-DIC ring-core measurements of relief strain can now be probed for any cubic material for which the stiffness coefficients are known in the above matrix. In order to illustrate the effect of anisotropy on the apparent computed residual stress, three materials were chosen. The first choice is Ni-base superalloy which is known to display significantly high anisotropy. The second is single crystal silicon which has moderate degree of anisotropy. Finally, an example of cubic material that is almost isotropic is aluminium and its alloys. In accordance with eq.(24), the stiffness matrix of each crystal can be described using only three independent coefficients C_{11}, C_{12} and C_{44}. The stiffness coefficients can be found in the literature [15] for Ni-base superalloy IN718 that was also the material studied in [16]. The elastic stiffness coefficients for Si and Al were also taken from the literature [17].

Since three parameters needed to describe the most general case of elasticity of cubic symmetry materials, there is one additional stiffness coefficient that arises compared to the isotropic case. The degree of elastic anisotropy for cubic structure materials is described quantitatively by the Zener anisotropy factor:

$$A = \frac{2C_{44}}{(C_{11} - C_{12})} = \frac{2(S_{11} - S_{12})}{S_{44}}. \quad (25)$$

The anisotropy factor assumes the value of unity for isotropic material (e.g. W). The deviation from this value represents the degree to which the crystal stiffness in a particular direction varies with orientation.

We wish to compare the stress values obtained taking into account the effect of anisotropy and the stress value that would arise on the basis of the assumption of materials isotropy. The use of highly local FIB-DIC micro-ring-core probes makes this consideration directly relevant in the context of polycrystalline alloys which in the absence of texture (preferred crystal orientation) can be thought of as macroscopically isotropic agglomerates [18]. The equivalent isotropic elastic properties of the polycrystalline IN718 were taken from sources [15, 19] in the literature, along with those for polycrystalline Si and Al [20].

The table below reports the stiffness coefficients and anisotropy factor values for single crystals in the local coordinates associated with the lattice unit cell, together with Young's modulus and Poisson's ratio for untextured polycrystals.

Results

The calculations of the stress from given input strains were carried out following the procedure described above for a collection of 8000 uniformly distributed random crystal orientations. For the purpose of representation, the numerical results were normalized with respect to one

particular stress component, namely, σ_{11}, that was computed based on the isotropic material assumption. The results are reported in the histogram graphs shown in Figure 2.

The table below reports the statistical measures of the results obtained in terms of mean value, median and the 95% confidence interval.

Discussion

The histograms show very significant spread of actual stress values around the value obtained using the simplifying assumption of material isotropy. The mean normalized stress component σ_{11} corresponds to unity. Furthermore, the mean value of the σ_{22} component in all cases corresponds to the isotropic polycrystal's Poisson's ratio.

As expected, the material with the highest anisotropy factor (IN 718) displays the broadest distribution of stress values. In fact, the uniaxial strain example shows the values of σ_{11} computed using the correct anisotropic relations a spread in the range that deviates by approximately ±0.40 from the mean isotropic value. In the case of silicon and aluminium the range half-width drops to around 0.16 and 0.08, respectively. It is worth noting that under the uniaxial strain state, the component of in-plane stress σ_{22} that is perpendicular to the applied strain direction may assume a negative value. This behavior is only observed in materials with a high anisotropy factor.

The equibiaxial strain state analysis confirms further that the spread of values is consistent with the anisotropy factor, i.e. the materials that display higher degree of anisotropy also show greater spread.

Regarding the third example of strain state, the observation that can be made is that in this case the stress component showing the highest magnitude does not always correspond to the component of strain with the highest magnitude. Therefore, particular care must be taken in interpreting the principal stress and orientation at a given location within the sample, if the underlying grain orientation is not known.

In general, the case that gives the widest range of stress value distribution is the uniaxial one, providing a basis for the 'worst case scenario' conservative estimation.

5. Experimental illustration

Experimental procedure

In this section an illustration of the relevance of the developed procedure is provided using a case study. A polished section of a component made from the Ni-base superalloy IN718 was carefully polished to avoid the introduction of additional residual stresses. The section was first ground using the 320 grit grinding paper. This was followed by grinding with papers of increasing grit size up to 4000 grit to improve the surface finish, and to remove the consequence of the previous step. Polishing of the surfaces was then performed using 0.1 μm diamond suspension. In total, ten FIB-DIC ring-core markers were milled on the surface along a straight line. The spacing was not uniform and ranged from 0.05mm for the points in the central zone, and 0.10mm for the points at the ends. The milling configuration is illustrated in Figure 3, superimposed over the

EBSD map that indicates grain orientation. The EBSD map was acquired following the milling procedure in order to determine the underlying crystal orientation at each milling location, with three triplets of Euler angles obtained at each position.

The milling procedure was performed using the ring-core procedure with a 5μm inner diameter and the trench width of 1μm. The FIB parameters used for the milling were: ion beam energy of 30 keV and ion beam current of 0.17nA. The milling process was subdivided into 50 incremental steps. At each step a high magnification SEM image was acquired at 5keV electron beam energy and 260nA electron current.

The two directions indicated in Figure 3 were assumed to be principal, and DIC analysis was performed for the strain components along these directions. As last step for the determination of relief strains, the DIC strain-depth curve was fitted with the master curve as described in [10].

Results

The spatially resolved profile of residual stress under isotropic material behaviour assumption was reconstructed, and is plotted in Fig.4. The preceding uncertainty analysis allowed the error to be induced that arises by ignoring the anisotropy, and using isotropic assumptions. This is represented in the graph using the upper and lower dotted profiles that delimit the 95% confidence interval. The direct comparison of results obtained taking into account the correct anisotropic elastic behaviour of the material is also reported in the Figure. The expected prevalent compressive residual stress state was found in the material, in both *x* and *y* directions, as is apparent from Fig.4.

Discussion

The consideration of the trends in the spatial variation of stresses computed using the isotropic and anisotropic assumptions reveals close similarity between the two approaches. The magnitude of the stresses, however, displays large deviations. The stress component in the *x* direction shows the greatest deviation from the isotropic calculation at the milling point no. 9. At this position the value given by the anisotropic elasticity calculation differs from the isotropic computation by about 33%. For the orthogonal direction of stress (the *y* component), the largest difference is observed at point no.4, where the offset is close to 25%.

Comparing the experimental results shown here with the examples from the previous section, the case closest to the experimental situations discussed here is the one illustrated in Figure 2c. In this example the strain state is non-equibiaxial, and the uncertainty due to ignoring the underlying anisotropy effect is ±38% for this material (IN718). The plot shows the limits of the 95% confidence interval indicating the upper and lower bounding stress values. Once the orientation is known, as in the presented example, the stress can be calculated more precisely, and the result is shown in Fig.4. The result lies within the expected range of variation predicted on the basis of isotropy assumption and uncertainty quantification.

6. Conclusions

The analysis of statistical variation and uncertainty of stress evaluation using FIB-DIC ring-core analysis in combination with anisotropic elasticity calculations has been presented. The widest range of stress values obtains in the instance when the state of strain is close to uniaxial.

As expected, the material with the highest anisotropy factor (IN 718) gives the broader distribution of possible stress. In the uniaxial strain state example it was found that the σ_{11}stress component could take values in a range centred around the isotropic calculation, but may deviate from this value by as much as ±40%. In the case of silicon and aluminium the largest deviation drops to around ±16% and ±8%, respectively.

An experimental illustration was provided that showed the application of the procedure to the situation when EBSD technique provides the knowledge of grain orientation at the measurement location. The results obtained are consistent with the expectations based on the statistical analysis of uncertainty.

Acknowledgement:

AMK acknowledges funding received for the MBLEM laboratory at Oxford through EU FP7 project iSTRESS (604646). The authors declare no conflict of interest.

References:

[1] Macherauch, E, 1984. Residual Stresses. Application of Fracture Mechanics to Materials and Structures, pp. 157-192

[2] Niku Lari, A, 1987. Advances in Surface Treatments, Technology-Applications-Effects, Int. Guidebook on Residual Stresses. Pergamon Press, Oxford, vol.4.

[3] Eshelby, J. D., 1957. The determination of the elastic field of an ellipsoidal inclusion. Proc. R. Soc. London, A 241, pp. 376- 396.

[4] Oliver, E.C., Daymond, M.R., Withers, P.J., 2004. Interphase and intergranular stress generation in carbon steels. Acta Materialia 52, pp.1937–1951.

[5] Korsunsky, A. M., Jarnes, K.E., Daymond, M.R., 2004. Intergranular stresses in polycrystalline fatigue: diffraction measurement and self-consistent modelling. Eng Fracture Mech. 71, pp. 805-812

[6] Clausen, B, Lorentzen, T., Leffers, T., 1998. Self-consistent modelling of the plastic deformation of f.c.c. polycrystals and its implications for diffraction measurements of internal stresses. Acta mater. Vol. 46, No. 9, pp. 3087-3098.

[7] Korsunsky, A.M., Sebastiani, M., Bemporad, E., 2009. *Focused ion beam ring drilling for residual stress evaluation*. Material Letters 63, pp.1961-1963.

[8] Song, X., Yeap, K.B., Zhu, J., Belnoue, J., Sebastiani, M., Bemporad, E., Zeng, K.Y., Korsunsky, A. M., 2011. Residual stress measurement in thin films using the semidestructive ring-core drilling method using Focused Ion Beam. Proc. Eng. 10, pp.2190–2195

[9] Lunt, A. J. G., Korsunsky, A. M., 2014. Intragranular Residual Stress Evaluation Using the Semi-Destructive FIB-DIC Ring-Core Drilling Method. Advanced Materials Research Vol 996, pp 8-13 doi:10.4028/www.scientific.net/AMR.996.8

[10] Korsunsky, A.M., Sebastiani, M., Bemporad, E, 2010. Residual stress evaluation at the micrometer scale: Analysis of thin coatings by FIB milling and digital image correlation. Surf. and Coat. Tech. Vol. 205, Issue 7, 25, pp. 2393–2403

[11] Zener, C., 1948. Elasticity and Anelasticity of Metals, University of Chicago. (1948) Press, Chicago.

[12] Costantinescu, A., Korsunsky, A.M., 2007. Elasticity with Mathematica. Cambridge University Press. ISBN 978-0-521-84201-3

[13] Bunge, H.J., 1969. Texture Analysis in Materials Science. Mathematical Methods. Elsevier Ltd. All rights reserved. ISBN: 978-0-408-10642-9

[14] Salvati, E., Lunt, A. J.G., Sui, T., Korsunsky, A. M., 2015. An Investigation of Residual Stress Gradient Effects in FIB-DIC Micro-Ring-Core Analysis. IMECS 2015, Hong Kong;

[15] Holden, T.M., Holt, R.A., Clarke, A.P., 1998. Intergranular strains in Inconel-600 and the impact on interpreting stress fields in bent steam-generator tubing. Material Science and Engineering A246, pp.180-198

[16] Tayon, W., Shenoy, R., Bird, R., Hafley, Redding, M., 2014. Texture-Induced Anisotropy in an Inconel 718 Alloy Deposited Using Electron Beam Freeform Fabrication. Int. Conf. on Texture of Materials; 17th; 24-29 Aug. 2014; Dresden; Germany

[17] Courtney, T., 2005. Mechanical Behavior of Materials. McGraw-Hill, 0-07-013265-8, 620.11292 C86M.

[18] Hutchinson, J.W., 1970. Elastic-plastic behaviour of polycrystalline metals and composites. Proc. Roy. Soc. Lond. A. 319, pp. 247-272

[19] Fukuhara, M., Sanpei, A., 1993. Elastic moduli and internal frictions of Inconel 718 and Ti-6AI-4V as a function of temperature. J. of Material Science Letters 12, pp. 1122-1124

[20] Hopcroft, M. A., Nix, W. D., Kenny, T. W., 2010. What is the Young's Modulus of Silicon. Journal Of Microelectromechanical Systems, Vol. 19, No. 2,

Figure Captions:

Fig.1. Cartesian Coordinate System definition at the ring core. The axes 1 and 2 denotes the in-plane coordinates and the axis 3 the out-of-plane coordinate. (a) Illustration of the evolution of the micro-scale ring-core geometry during Focused Ion Beam (FIB) milling. The diameter of the central pillar is 5μm. (b) Coordinate systems defined as global (G) (associated with laboratory axes) and local (L) (associated with sample crystal axes) for a single crystal micro-pillar.

Fig. 2 Distribution of the evaluated stresses $\sigma_{11}$and σ_{22} in case of anisotropic material for IN718, Si and Al materials. a) Uniaxial strain state. b) Equibiaxial strain state c) Non-equibiaxial strain state.

Fig.3 EBSD Inverse Pole Figure map and milling point locations.

Fig. 4 Residual stress profiles and comparison between hypothesis of Isotropic and Anisotropic material. The region within the two dotted lines represents the confidence interval in which the stress value may lie considering anisotropy at 95% confidence interval. a) Component of residual stress in x direction $\sigma_{res,xx}$. b) Component of residual stress in y direction $\sigma_{res,yy}$.

a). 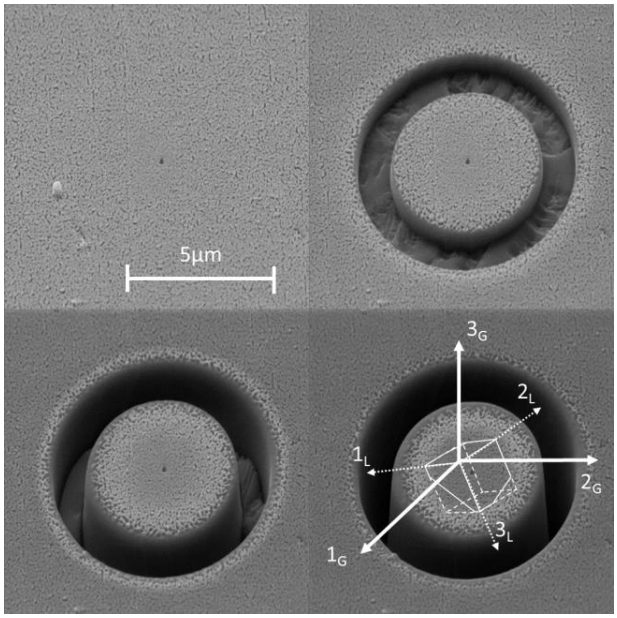

b). 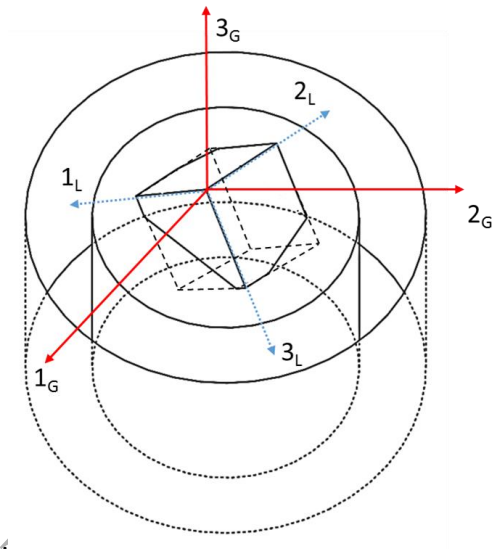

Fig.1. Cartesian Coordinate System definition at the ring core. The axes 1 and 2 denotes the in-plane coordinates and the axis 3 the out-of-plane coordinate. (a) Illustration of the evolution of the micro-scale ring-core geometry during Focused Ion Beam (FIB) milling. The diameter of the central pillar is 5µm. (b) Coordinate systems defined as global (G) (associated with laboratory axes) and local (L) (associated with sample crystal axes) for a single crystal micro-pillar.

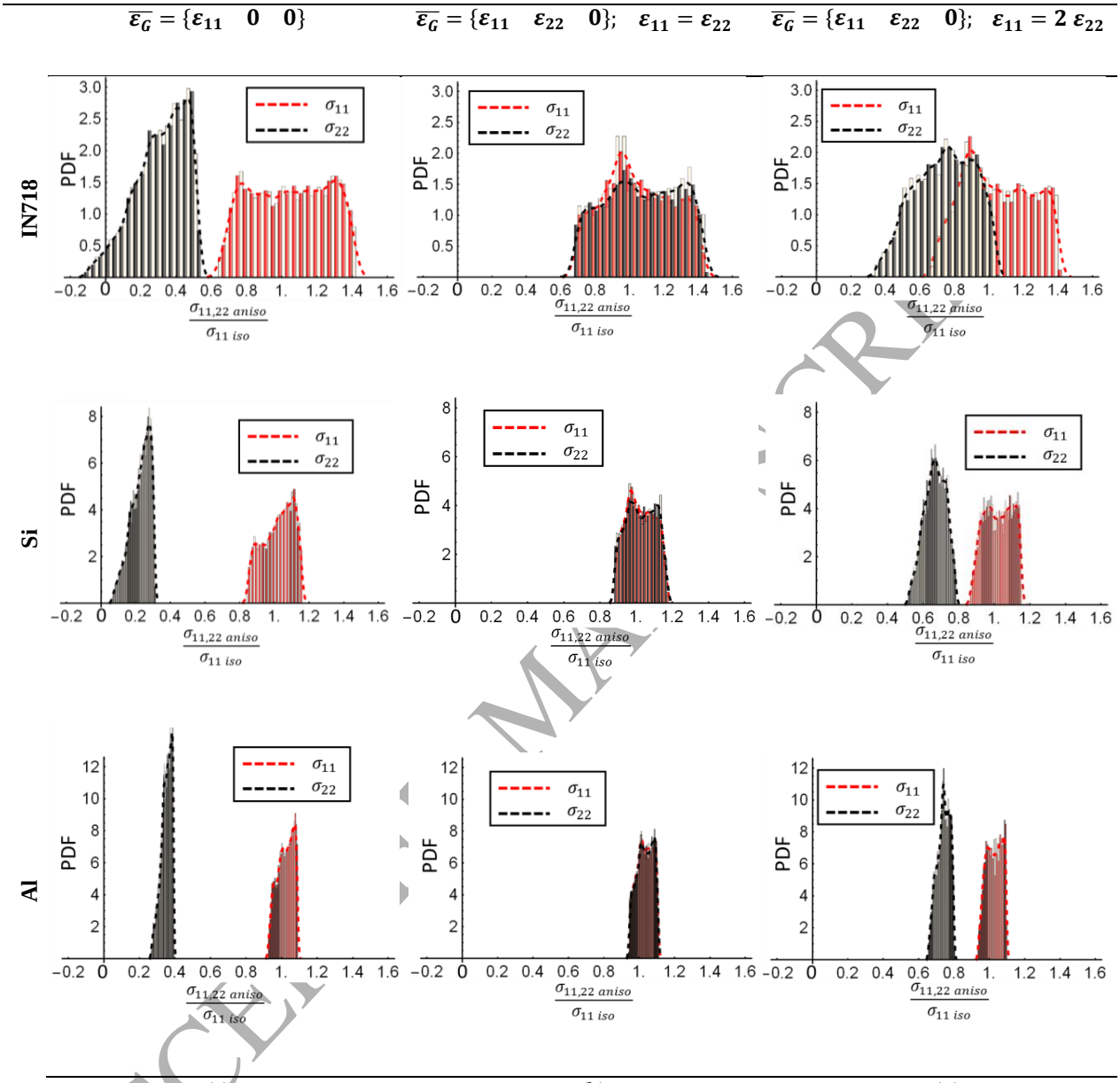

Fig. 2 Probability Distribution Functions (PDF) of the evaluated stresses σ_{11} and σ_{22} in case of anisotropic material for IN718, Si and Al materials. a) Uniaxial strain state. b) Equibiaxial strain state c) Non-equibiaxial strain state.

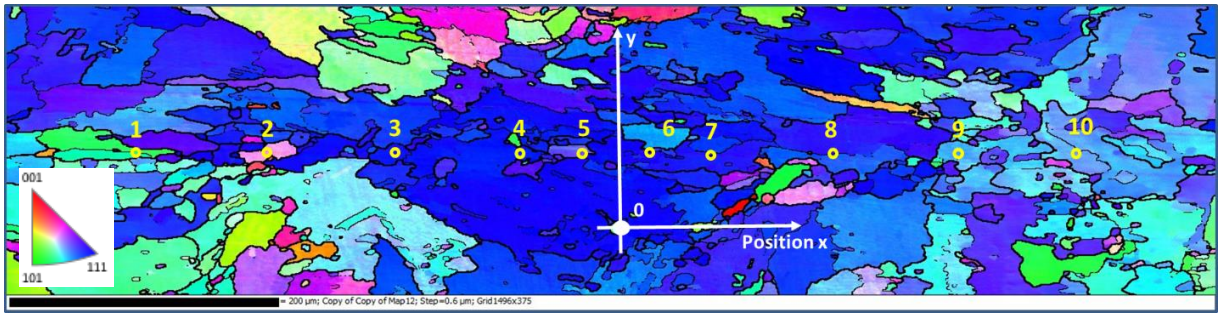

Fig.3 EBSD Inverse Pole Figure map and milling point locations.

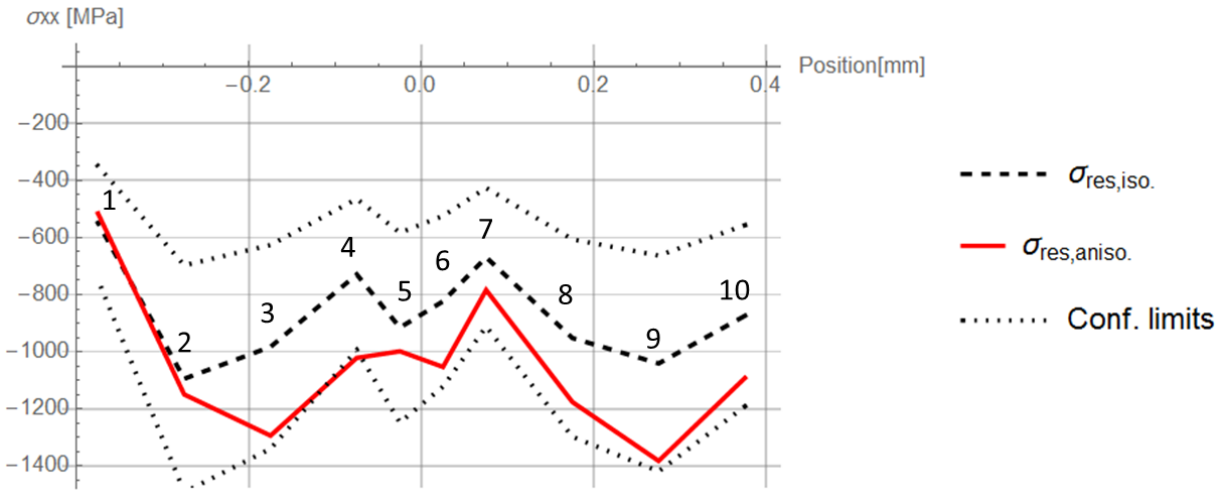

(a)

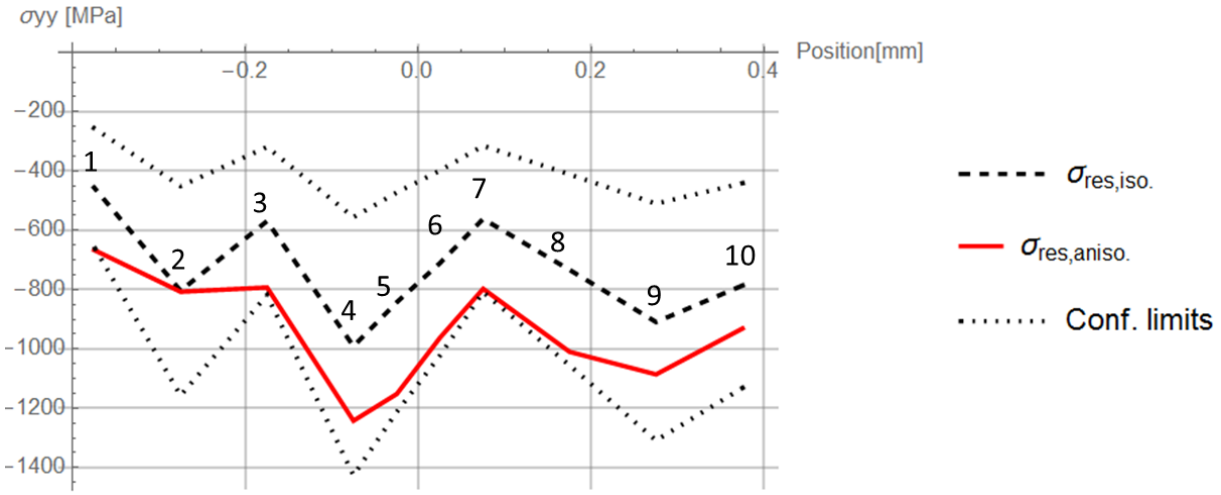

(b)

Fig. 4 Residual stress profiles and comparison between hypothesis of Isotropic and Anisotropic material. The region within the two dotted lines represents the confidence interval in which the stress value may lie considering anisotropy at 95% confidence interval. a) Component of residual stress in x direction $\sigma_{res,xx}$. b) Component of residual stress in y direction $\sigma_{res,yy}$.

Tab.1 Elastic stiffness coefficients of selected materials with cubic elastic symmetry

Material	C_{11} [MPa]	C_{12} [MPa]	C_{44} [MPa]	A	E_{poly} [MPa]	ν_{poly}
IN718	234600	145400	126200	2.83	206000	0.29
Si	166000	64000	80000	1.57	160000	0.22
Al	108000	61000	29000	1.23	71000	0.33

Tab. 2 Statistical results. The value of β indicates the 95% confidence interval.

Mat.	CASE	$\left(\frac{\sigma_{11,anis}}{\sigma_{11,iso}}\right)_{mean}$	$\left(\frac{\sigma_{22,anis}}{\sigma_{11,iso}}\right)_{mean}$	$\left(\frac{\sigma_{11,anis}}{\sigma_{11,iso}}\right)_{med.}$	$\left(\frac{\sigma_{22,anis}}{\sigma_{11,iso}}\right)_{med.}$	$\left(\frac{\sigma_{11,anis}}{\sigma_{11,iso}}\right)_{St.Dev.}$	$\left(\frac{\sigma_{22,anis}}{\sigma_{11,iso}}\right)_{St.Dev.}$	$\beta_{\sigma_{11,anis}}$	$\beta_{\sigma_{22,anis}}$
Ni	***a***	1.048	0.312	1.052	0.332	0.212	0.143	±0.40	±0.90
	b	1.055	1.075	1.036	1.073	0.197	0.210	±0.36	±0.38
	c	1.052	0.742	1.038	0.751	0.195	0.166	±0.36	±0.44
Si	***a***	1.021	0.085	1.032	0.237	0.085	0.056	±0.16	±0.49
	b	1.023	1.027	1.019	1.027	0.076	0.079	±0.15	±0.15
	c	1.022	0.666	1.023	0.669	0.076	0.060	±0.15	±0.18
Al	***a***	1.021	0.351	1.024	0.356	0.044	0.029	±0.08	±0.16
	b	1.032	1.033	1.033	1.034	0.044	0.044	±0.08	±0.08
	c	1.027	0.740	1.028	0.743	0.043	0.035	±0.08	±0.08

Vitae:

Mr. Enrico Salvati is a second-year DPhil candidate founded by EU FP7 collaborative research project iSTRESS. Enrico is also a Trinity College member and Visiting Staff member at the Research Complex at Harwell (UK). His reseach interest concerns the development of FIB-DIC micro ring core for the evaluation of residual stress, quantification of residual stress ahead crack tip using hi-resolution Synchrotron Powder Diffraction and FIB-FIC, Fatigue in metallic material and Finite Element Modelling.

Dr. Tan Sui is currently Postdoctoral Researcher under EU FP7 collaborative research project iSTRESS on FIB-DIC residual stress analysis at the micro-nano-scale. She is Visiting Staff member at the Research Complex at Harwell, and College Tutor in Engineering Science at St Anne's College, Oxford. She is Managing Editor for *Materials & Design* (Elsevier). Her research interests concern microstructural characterization and multi-scale modelling of thermo-mechanical behaviour of hierarchically structured materials and tissues using multi-modal X-ray techniques (Diffraction, Imaging and Spectroscopy), as well as multi-beam microscopy techniques (FIB, SEM, EDX, EBSD, STEM and TOF-SIMS).

Prof. Alexander M. Korsunsky is a world-leader in engineering microscopy of materials and structures for optimisation of design, durability and performance. He heads Multi-Beam

Laboratory for Engineering Microscopy (MBLEM) at Oxford, and Centre for In situ Processing Science (CIPS) at Research Complex at Harwell. He consults Rolls-Royce plc on residual stress and structural integrity, and is Editor-in-Chief of *Materials & Design*, a major Elsevier journal (2014 IF 3.501). Korsunsky's group research interests concern improved understanding of integrity and reliability of engineered and natural structures, from high-performance metallic alloys to polycrystalline ceramics to natural hard tissue such as human dentin and seashell nacre.

Graphical Abstract